PAPER • OPEN ACCESS

A study on multi-GNSS phase-only positioning

To cite this article: A Khodabandeh *et al* 2021 *Meas. Sci. Technol.* **32** 095005

View the article online for updates and enhancements.

A study on multi-GNSS phase-only positioning

A Khodabandeh[1,*] , S Zaminpardaz[2] and N Nadarajah[3]

[1] Department of Infrastructure Engineering, The University of Melbourne, Melbourne, Australia
[2] School of Science, RMIT University, Melbourne, Australia
[3] Locata Corporation, Canberra, Australia

E-mail: akhodabandeh@unimelb.edu.au

CrossMark

Abstract

The global navigation satellite systems (GNSS) carrier phase measurements form the basis of high-precision satellite positioning. These measurements are often accompanied by their code counterparts to enable one to compute single-epoch ambiguity-resolved positioning solutions. To avoid unwanted code modelling errors, such as code multipath, one may opt for a phase-only solution and take recourse to carrier phase measurements of two successive epochs. In this paper we study the ambiguity resolution performance of a dual-epoch phase-only model, upon which the unknown positioning parameters are assumed to be completely unlinked in time. With the aid of closed-form analytical results, it is investigated how ambiguity resolution performs when dealing with high-rate phase data. It is thereby shown that multi-GNSS integration makes near real-time centimetre-level phase-only positioning possible. Our analytical analysis is supported by means of numerical results.

(Some figures may appear in colour only in the online journal)

1. Introduction

Global navigation satellite systems (GNSS) have been widely used as an effective means of delivering ubiquitous positioning and navigation services. While the pseudo-range (code) measurements form the basis of GNSS standard positioning, it is the provision of their carrier phase counterparts that leads to ultra precise positioning solutions, see e.g. Blewitt (1989), Remondi (1989), Teunissen (1995), Tiberius and de Jonge (1995), Jonkman *et al* (2000), Hauschild *et al* (2008), Gunther and Henkel (2012), and Odolinski *et al* (2015). This is because the GNSS carrier phase measurements are, approximately, two orders of magnitude more precise than the code measurements. The starring role of carrier phase measurements in GNSS positioning is particularly pronounced when their unknown ambiguities are successfully resolved to their integer values using methods of integer ambiguity resolution (Teunissen 1995, Han 1997, Hassibi and Boyd 1998, Xu *et al* 2012, Khodabandeh and Teunissen 2018). Once the ambiguities are resolved, the carrier phase measurements will act as ultra precise code measurements, thus making fast and precise positioning and navigation possible. Integer ambiguity resolution is therefore considered to be the key to fast and precise GNSS parameter estimation. Next to GNSS, integer ambiguity resolution has also found a widespread usage in other interferometric techniques, such as very long baseline interferometry (Hobiger *et al* 2009), interferometric synthetic aperture radar (Kampes and Hanssen 2004), or underwater acoustic carrier phase positioning (Viegas and Cunha 2007).

In real-time positioning applications where only a *single* epoch of GNSS data is utilised, carrier phase measurements have to be accompanied by code measurements to make the

---

* Author to whom any correspondence should be addressed.

underlying model solvable for the to-be-resolved phase ambiguities. However, if data of multiple epochs are considered, one can exploit the change in the satellite geometry and deliver *phase-only* solutions (Teunissen 1997a). The main advantage of phase-only positioning over its phase-and-code version is that unwanted code modelling errors, such as code multipath, can be avoided (Remondi and Brown 2000, Codol and Monin 2011). In (ibid), ambiguity resolution was not considered and phase-only models were only used to compute positioning solutions. As a consequence, a rather long observation time-span (∼1 h) is required to obtain centimetre-level solutions. To shorten the stated time-span, Teunissen *et al* (1997) introduced the principle of phase-only ambiguity resolution. Recent contributions have demonstrated that relatively fast phase-only ambiguity-resolved positioning (∼10–30 s) is indeed feasible (Huisman *et al* 2010, Wang *et al* 2018).

To realise fast phase-only positioning, Wang *et al* (2018) studied the ambiguity-resolution performance of GPS triple-frequency for short baselines. It was shown that millimetre-level positioning can be achieved by using only *two* successive epochs of phase data. In the aforementioned contributions, phase-only positioning is based on a rather stringent assumption in that the baseline parameters are assumed to behave *unchanged* in time. It is therefore the goal of the present contribution to address whether such assumption is really needed, particularly, for a multi-GNSS setup where GNSS receivers track a large number of satellites, collecting large amounts of phase data on multiple frequencies. To this end, we study the ambiguity resolution performance of a *dual-epoch* phase-only model upon which the unknown baselines are treated as *fully* unlinked-in-time parameters. It is investigated how ambiguity resolution performs when dealing with *high-rate* multi-GNSS data, e.g. with 5 Hz or 1 Hz sampling-rates.

The remainder of this paper is organised as follows. Section 2 is devoted to the GNSS short-baseline model on which our analysis is based. Closed-form expressions for the variance matrices of the model's parameter solutions are derived and the prominent role of multi-GNSS integration in achieving successful ambiguity-resolution is highlighted. In section 3, we study the phase-only ambiguity resolution performance using the concept of ambiguity dilution of precision (ADOP) (Teunissen 1997a), thereby quantifying the impact the measurement sampling-rate has on the model's ambiguity resolution strength. In section 4, real-world multi-GNSS data-sets, of different sampling-rates, are analysed to provide numerical insights into the positioning performance of the proposed dual-epoch phase-only model. Finally, concluding remarks are provided in section 5.

We make use of the following notation. The *n*-dimensional space of real numbers is denoted by $\mathbb{R}^n$, while the *n*-dimensional space of integers is denoted by $\mathbb{Z}^n$. The identity matrix and vector of ones are denoted by *I* and *e*, respectively. $\mathsf{E}(\cdot)$ denotes the mathematical expectation operator. The capital *Q* is reserved for (co)variance matrices, with Q_{xy} being the $n \times p$ covariance matrix of two random vectors $x \in \mathbb{R}^n$ and $y \in \mathbb{R}^p$. Thus Q_{xx} indicates the variance matrix of *x*. The transpose of a matrix is shown by the superscript *T*, i.e. $(\cdot)^T$. To express closed-form analytical results in a compact manner,

the Kronecker matrix product ⊗ is employed (Henderson *et al* 1983).

2. The dual-epoch kinematic phase-only model

In this section we discuss the GNSS short-baseline model on which our analysis is based. The precision of the parameter solutions, obtained by such model, is quantified and the prominent role taken by the multi-GNSS integration in increasing the model's ambiguity success-rate is pointed out.

2.1. Double-differenced observation equations

Let $\Delta\phi_i \in \mathbb{R}^{f(m-1)}$ denote the vector of double-differenced (DD) observed-minus-computed carrier phase measurements that are collected by two GNSS receivers tracking *m* common satellites, on *f* frequencies, at epoch *i* ($i = 1, 2$). The distance between the two receivers is assumed short enough so that the DD atmospheric delays can be neglected. With these in mind, the corresponding linearised observation equations read (Teunissen 1997b, Khodabandeh and Teunissen 2018)

$$\mathsf{E}(\Delta\phi_i) = [\Lambda \otimes I]\,a + [e \otimes G_i]\,\Delta b_i \quad (1)$$

where the unknown DD ambiguities $a \in \mathbb{Z}^{f(m-1)}$ are linked to the measurements through the $f \times f$ diagonal matrix $\Lambda = \text{diag}(\lambda_1, \ldots, \lambda_f)$, with λ_j being the wavelength of the phase data on frequency *j* ($j = 1, \ldots, f$). The 3-vector Δb_i contains the unknown increments of the three-dimensional baseline b_i at epoch *i*. The corresponding $(m-1) \times 3$ coefficient matrix is indicated by $G_i = D_m^T A_i$ and is assumed full-rank, where the $m \times 3$ matrix A_i contains the receiver-satellite direction vectors. The $m \times (m-1)$ matrix D_m forms between-satellite differences. The orbital corrections are assumed applied to the observed-minus-computed measurements. In the above equations and in the following, the epoch subscript *i* is used to emphasise the time dependency of the quantities. In the case of the DD ambiguities *a* however, the subscript *i* is omitted. This is because the phase ambiguities are constant in time if no cycle slips occur. It is also important to remark that code data are used to compute the approximate values needed for linearising the observation equations.

Why two epochs: If we stick to only one *single* epoch of phase data, the system of equations (1) would then be under-determined as there are $f(m-1)$ equations in $f(m-1)+3$ unknowns, i.e. $f(m-1)$ ambiguities plus three baseline components. The rank-defect is 3. Assuming that the augmented matrix $[G_1, G_2]$ is of full column rank, at least two epochs of phase data are required to have the model (1) solvable for the unknowns *a* and $\Delta b_i (i = 1, 2)$. Under such assumption, the solvability condition of (1) is given by

$$m \geq 7. \quad (2)$$

Thus phase data of a minimum number of seven satellites is needed. Although phase data of more than two epochs can also be considered, here we confine our study to a two-epoch scenario as it has the potential to realise near real-time phase-only positioning when dealing with *high-rate* GNSS data, e.g.

with 5 Hz or 1 Hz sampling-rates. It should be remarked, for a single-GNSS setup and under unfavourable measurement conditions like urban canyons, that the solvability condition (2) may not always hold (Montenbruck *et al* 2017).

Why kinematic: In the literature, the phase-only model (1) has been studied under the assumption that the baseline parameters are *static* over time, i.e. $b_1 = b_2$, see e.g. (Tiberius and de Jonge 1995, Huisman *et al* 2010, Wang *et al* 2018). In the present contribution, we relax this stringent assumption and treat the baselines as *fully* unlinked-in-time parameters. In other words, no restriction is placed on the temporal behaviour of the two baseline vectors $b_i (i = 1, 2)$. The strength of such 'kinematic' model is less than that of its 'static' counterpart in the sense that it has *three more* unknowns (i.e. the baseline vector of the second epoch). Our goal is therefore to verify whether or not the stated weakness of the kinematic model (1) is of practical relevance for a multi-GNSS landscape where positioning users can track a large number of satellites ($\sim$20), collecting large amounts of phase data on multiple frequencies.

2.2. Precision of the baseline solutions

In order to evaluate the variance matrices of the parameter solutions obtained by (1), the stochastic model of the DD phase measurements $\Delta\phi_i$ $(i = 1, 2)$ is assumed given as (Khodabandeh and Teunissen 2015a)

$$Q_{\phi_i\phi_i} = 2\sigma_\phi^2 [I \otimes W_i^{-1}], \quad i = 1, 2$$
$$Q_{\phi_1\phi_2} = 0 \tag{3}$$

where $W_i = (D_m^T C D_m)^{-1}$, with the $m \times m$ diagonal co-factor matrix $C = \text{diag}(w_1^{-1}, \ldots, w_m^{-1})$ whose positive elements w_s $(s = 1, \ldots, m)$ are the satellite elevation-dependent weights. The zenith-referenced standard deviation of the *undifferenced* phase measurements is denoted by σ_ϕ. The factor '2' in (3) indicates that the variance of the phase measurements is doubled by forming between-receiver differences. According to the second expression of (3), time correlation between the phase measurements $\Delta\phi_i$ $(i = 1, 2)$ is assumed to be absent.

We first present the variance matrix of the parameters of interest, i.e. the baseline parameters, for which we distinguish the following two cases:

- *Ambiguity-float*: the case that the DD ambiguities are unknown;
- *Ambiguity-fixed*: the case that the DD ambiguities are successfully resolved as integers.

Lemma 1 (Lemma.). (Phase-only baseline precision) *Let $\hat{b}_i$ and $\check{b}_i$, respectively, be the least-squares ambiguity-float and -fixed solutions of the baseline parameters b_i as given in (1). Their respective variance matrices can be given as*

$$Q_{\hat{b}_i\hat{b}_i} = Q_{\check{b}_i\check{b}_i} + \frac{2\sigma_\phi^2}{f} G_i^+ Q_{\hat{\rho}\hat{\rho}} G_i^{+T}, \quad i = 1, 2$$
$$Q_{\check{b}_i\check{b}_i} = \frac{2\sigma_\phi^2}{f} (G_i^T W_i G_i)^{-1}, \quad i = 1, 2 \tag{4}$$

where $Q_{\hat{\rho}\hat{\rho}} = (\sum_{i=1}^{2} W_i \mathcal{P}_{G_i}^\perp)^{-1}$, *with the projector* $\mathcal{P}_{G_i}^\perp = I - G_i G_i^+$. *The least-squares inverse of G_i is given by* $G_i^+ = (G_i^T W_i G_i)^{-1} G_i^T W_i$.

Proof. The proof is given in the appendix. $\qquad\square$

From the expressions (4), one can infer the precision of the baseline solutions obtained by the phase-only model (1). Let us first consider the second expression in which the DD ambiguities are assumed to be fixed to their integers. The variance matrix $Q_{\check{b}_i\check{b}_i}$ is driven by the precision of the phase data σ_ϕ, the number of frequencies f and the receiver-satellite geometry through the co-factor matrix $(G_i^T W_i G_i)^{-1}$. The latter is identical to the co-factor of the code-based baseline positioning (Teunissen 1997a), meaning that $Q_{\check{b}_i\check{b}_i}$ is just a downscaled version of its code-based counterpart. Considering that the precision of code-based short-baseline positioning is at the metre-level and that the phase data are almost two orders of magnitude more precise than the code data, the precision of the phase-only ambiguity-fixed solutions $\check{b}_i$ $(i = 1, 2)$ is at the millimetre to centimetre level. Achieving such high-precision solutions relies on the assumption that one successfully maps the unknown ambiguities a to their correct integers, thus requiring an application of ambiguity resolution (Teunissen 1995).

Before applying ambiguity resolution, one should, however, first investigate whether it is worthwhile to do so as the phase-only ambiguity-float solutions $\hat{b}_i$ may already inherit the high-precision of their ambiguity-fixed versions $\check{b}_i$. In the first expression of (4), the ambiguity-float variance matrix $Q_{\hat{b}_i\hat{b}_i}$ is written as the sum of its ambiguity-fixed counterpart $Q_{\check{b}_i\check{b}_i}$ and the positive-definite matrix $(2\sigma_\phi^2/f)G_i^+ Q_{\hat{\rho}\hat{\rho}} G_i^{+T}$. The latter, in its turn, is driven by the co-factor matrix $Q_{\hat{\rho}\hat{\rho}}$. The inverse of the co-factor matrix $Q_{\hat{\rho}\hat{\rho}}$ is formed as a 'weighted sum' of the projectors $\mathcal{P}_{G_i}^\perp$ $(i = 1, 2)$. This implies, when $G_2 \approx G_1$, that the inverse-matrix $Q_{\hat{\rho}\hat{\rho}}^{-1}$ is near rank defect (near singular). This is because the projectors are singular matrices (Teunissen *et al* 2005). In such cases, the entries of $Q_{\hat{\rho}\hat{\rho}}$ are rather large, indicating that the ambiguity-float solutions $\hat{b}_i$ are *poorly* estimable. Unfortunately, the approximation $G_2 \approx G_1$ holds true for high-rate GNSS data as the receiver-satellite geometries change rather slowly in time. This is due to the high-altitude orbits of the GNSS satellites. The higher the sampling rate, the closer the approximation $G_2 \approx G_1$, thereby the poorer the precision of the solutions $\hat{b}_i$ becomes.

To address to what extent the precision of the ambiguity-float baseline solutions is poorer than their fixed versions, we use the concept of *gain numbers* (Teunissen 1997a). The gain numbers tell us how many times the variance of a function of the baseline solution $\hat{b}_i$ gets smaller after ambiguity-fixing. Since different functions of the baseline can have distinct responses to ambiguity resolution, we employ the average precision gain $\bar{\gamma}$ defined as follows

$$\bar{\gamma} = \left(\frac{|Q_{\hat{b}_i\hat{b}_i}|}{|Q_{\check{b}_i\check{b}_i}|} \right)^{1/3} \tag{5}$$
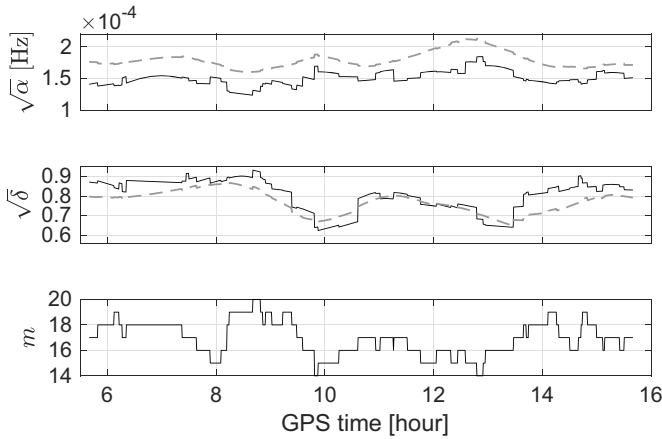
Figure 1. Time-series of the positive scalars $\sqrt{\alpha}$ (top) and $\sqrt{\delta}$ (middle) as given in (6), together with the corresponding number of satellites (bottom) for a GPS+Galileo data-set, cf. figure 3. The black solid lines correspond to the elevation weights $w_s = 1$, while the grey dashed lines correspond to the elevation-dependent weights given in (18).

in which $|\cdot|$ denotes the determinant of a matrix. The following lemma shows the dependency of $\bar{\gamma}$ on the sampling-rate of the phase measurements.

Lemma 2 (Lemma.). (Average precision gain) *Let τ be the measurement sampling period, i.e. the reciprocal of the sampling rate. Also let the $m \times 3$ matrix $\dot{A}$ contain the time-derivatives of the entries of $(1/2) \sum_{i=1}^{2} A_i$ in (1), with $W_2 \approx W_1 = W$. Using the first-order approximation $A_2 - A_1 \approx \tau \dot{A}$ for small values of τ, the average precision gain of the phase-only baseline solutions can be approximated by*

$$\bar{\gamma} \approx \left(\prod_{k=1}^{3} \left[1 + \frac{4}{\alpha_k \tau^2} \right] \right)^{1/3} \times \frac{\left(\prod_{k=1}^{3} \left[1 + \frac{\alpha_k \tau^2}{4} \right] \right)^{1/3}}{\left(\prod_{k=1}^{3} [1 - \beta_k] \right)^{1/3}}$$

$$\approx \frac{4}{\alpha \, \delta \, \tau^2} \tag{6}$$

with $\alpha = \left(\prod_{k=1}^{3} \alpha_k \right)^{1/3}$ and $\delta = \left(\prod_{k=1}^{3} [1 - \beta_k] \right)^{1/3}$, where the eigenvalues α_k and β_k are, respectively, the roots of the characteristic equations

$$\begin{aligned} |(\dot{G}^T W \dot{G}) - \alpha_k (G^T W G)| = 0, &\qquad k = 1, 2, 3 \\ |(G^T W \mathcal{P}_{\dot{G}} G) - \beta_k (G^T W G)| = 0, &\qquad k = 1, 2, 3 \end{aligned} \tag{7}$$

with $G = (1/2) \sum_{i=1}^{2} G_i$, $\dot{G} = D_m^T \dot{A}$, and the projector $\mathcal{P}_{\dot{G}} = \dot{G}(\dot{G}^T W \dot{G})^{-1} \dot{G}^T W$.

Proof. The proof is given in appendix. $\qquad \square$

Thus the average precision again $\bar{\gamma}$ is almost *inversely* proportional to the squared sampling period τ^2 and the positive scalars α and δ. To get some insight into (6), we present time-series of $\sqrt{\alpha}$ and $\sqrt{\delta}$ in figure 1. While the scalar $\sqrt{\alpha}$ is of the order of 10^{-4} Hz, the scalar $\sqrt{\delta}$ varies between 0.6 to 1. This implies, for small values of τ, that

$$\sqrt{\bar{\gamma}} \propto \frac{1}{\tau} 10^4 \tag{8}$$

in which τ is in *seconds* and the symbol $\propto$ means 'is of the order of'. The square-root gain $\sqrt{\bar{\gamma}}$ indicates how many times the standard deviation of the ambiguity-float baseline solutions is roughly larger than its fixed version. Accordingly, when 1 Hz phase measurements are considered ($\tau = 1$ s), the precision of the phase-only ambiguity-float solutions $\hat{b}_i$ is expected to be about tens of metres, i.e. 10^4 times millimetres. By increasing the sampling period to 10 s (i.e. $\tau = 10$ s), the stated precision improves to several metres which is still way poorer than the sub-centimetre precision of the phase-only fixed solutions $\check{b}_i$.

2.3. Role of the multi-GNSS integration

That the phase-only model (1) delivers poorly estimable ambiguity-float baseline solutions may make one inclined to conclude that the model is not applicable to fast precise positioning. This would indeed be the case if successful ambiguity resolution is not realised. The decision whether or not ambiguity resolution is successful is determined by the probability of correct integer estimation, the so-called ambiguity *success-rate* (Teunissen 1999). The maximum possible success-rate, i.e. the integer least-squares (ILS) success-rate, is governed by the ambiguity variance matrix $Q_{\hat{a}\hat{a}}$. Assuming normally-distributed phase measurements, the ILS success-rate is given by the multivariate integral (ibid)

$$\text{success-rate} = \int_{S_0} \frac{1}{\sqrt{|2\pi Q_{\hat{a}\hat{a}}|}} \exp\left(-\frac{1}{2} ||x||_{Q_{\hat{a}\hat{a}}}^2 \right) \mathrm{d}x \tag{9}$$

in which the ILS pull-in region S_0 is characterised as

$$S_0 = \{ x \in \mathbb{R}^{f(m-1)} \,|\, ||x||_{Q_{\hat{a}\hat{a}}}^2 \leq ||x-z||_{Q_{\hat{a}\hat{a}}}^2, \, \forall z \in \mathbb{Z}^{f(m-1)} \} \tag{10}$$

with the notation $||\cdot||_{Q_{\hat{a}\hat{a}}}^2 = (\cdot)^T Q_{\hat{a}\hat{a}}^{-1} (\cdot)$. According to (9), one only needs the ambiguity variance matrix $Q_{\hat{a}\hat{a}}$ as input to evaluate the ILS success-rate. We therefore present a closed-form expression of $Q_{\hat{a}\hat{a}}$ for the phase-only model (1).

Lemma 3 (Lemma.). (Phase-only ambiguity precision) *Let $\hat{a}$ be the least-squares solution of the ambiguity parameters a as given in (1). Then, the ambiguity variance matrix can be given as*

$$Q_{\hat{a}\hat{a}} = \sigma_\phi^2 [\Lambda^{-1} \mathcal{P}_e^\perp \Lambda^{-1} \otimes W^{-1}] + 2\sigma_\phi^2 [\Lambda^{-1} \mathcal{P}_e \Lambda^{-1} \otimes Q_{\hat{\rho}\hat{\rho}}] \tag{11}$$

with $W = (1/2) \sum_{i=1}^{2} W_i$ and the projectors $\mathcal{P}_e = (1/f) e e^T$ and $\mathcal{P}_e^\perp = I - \mathcal{P}_e$.

Proof. The proof is given in appendix. $\qquad \square$

As with the float baseline variance matrices (4), the ambiguity variance matrix $Q_{\hat{a}\hat{a}}$, in (11), also contains the near rank defect co-factor matrix $Q_{\hat{\rho}\hat{\rho}}$. Does this indicate that successful ambiguity resolution is not feasible? To answer

Table 1. Formal integer least-squares success-rates (%), delivered by the phase-only model (1), as function of the sampling period τ and the number of visible satellites m for single-frequency (SF) and dual-frequency (DF) scenarios of a GPS+Galileo data-set. The bold values indicate successful ambiguity resolution.

	$m = 7$ SF/DF	$m = 10$ SF/DF	$m = 15$ SF/DF	$m = 20$ SF/DF
$\tau = 0.2$ s (5 Hz)	0.00/0.94	0.00/97.35	30.52/99.99	95.61/**100**
$\tau = 1.0$ s (1 Hz)	0.00/16.36	0.52/99.91	83.28/**100**	99.74/**100**
$\tau = 10.0$ s (0.1 Hz)	0.00/88.95	37.80/99.99	99.85/**100**	**100**/**100**
$\tau = 30.0$ s (0.03 Hz)	0.03/99.26	84.86/**100**	99.99/**100**	**100**/**100**
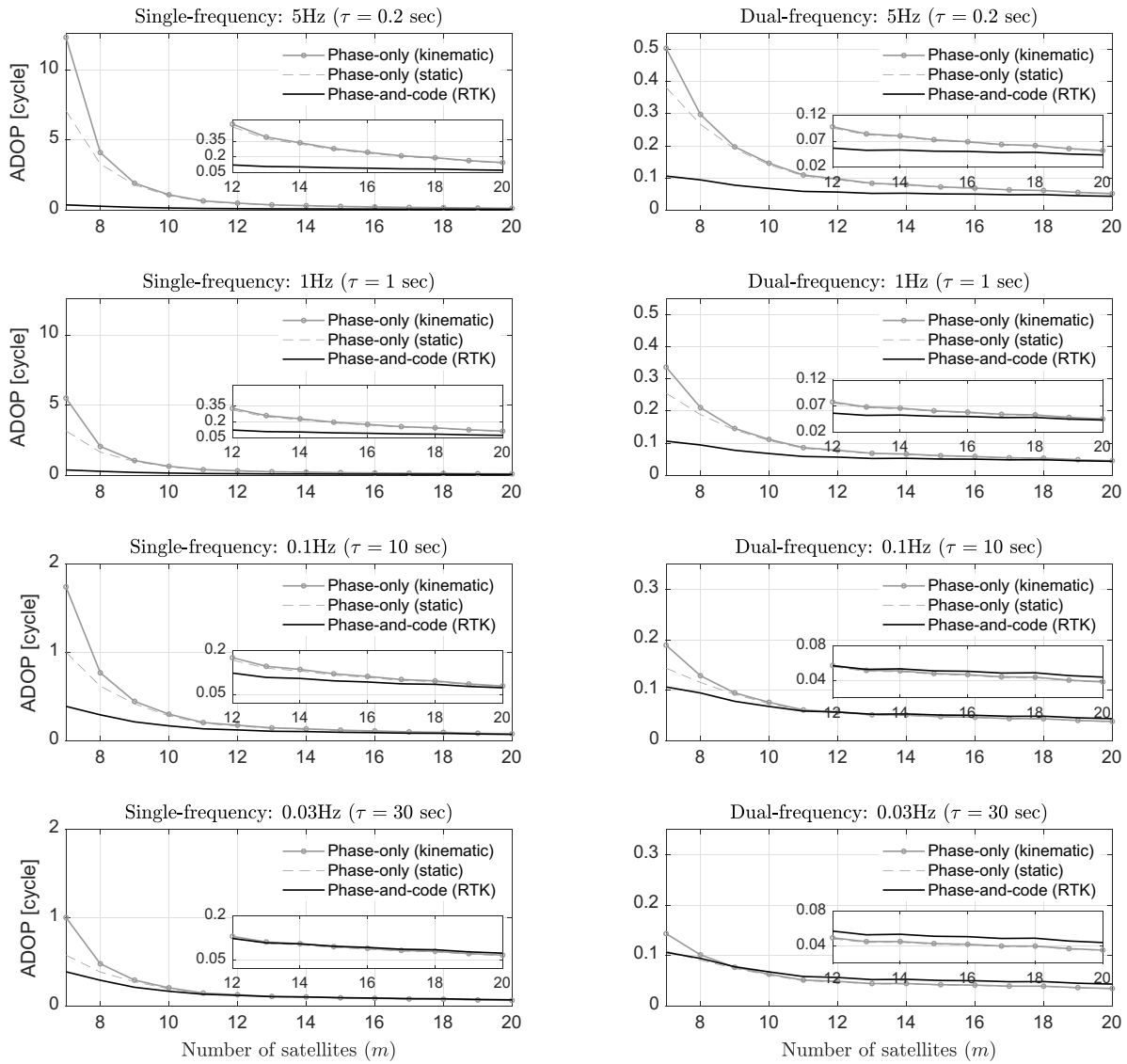
Figure 2. ADOPs corresponding to the phase-and-code RTK model (black lines), and of the phase-only kinematic (grey solid lines) and static (grey dashed lines) models as functions of the number of satellites m for different sampling periods τ.

this question, we use the Ps-LAMBDA software (Verhagen *et al* 2013) to numerically evaluate the multivariate integral (9) for a GPS-plus-Galileo scenario. The corresponding ILS success-rates are presented in table 1. The results are shown for different sampling periods τ and numbers of satellites m. The single- and dual-frequency cases refer to the L1(E1) and L1/L5(E1/E5a) signal frequencies, respectively.

When a minimum number of satellites ($m = 7$) is considered, the single-frequency success-rates are almost zero, while the dual-frequency success-rates can be larger than 99% *only* for the low-rate scenario of $\tau = 30$ s. Upon increasing the number of tracked satellites to $m = 20$ however, the dual-frequency success-rates can become almost 100% for even *high-rate* scenarios of $\tau = 0.2$ and 1 s. This highlights the important

Figure 3. Baseline CUT0–UWA0 located in Perth, Australia: [Left] UWA0 station; [Middle] baseline configuration (Map data @ 2020 Google); [Right] CUT0 station.

role played by the number of satellites, and therefore by the multi-GNSS integration, in delivering successful ambiguity-resolved solutions using the phase-only model (1). This notion will be made precise in the following section.

3. ADOP-analysis

So far we have learned that an increase in the number of tracked satellites can lead to almost 100% ambiguity success-rate for the dual-epoch phase-only model (1). Interestingly, this even holds true for *high-rate* phase data. In this section we further study the ambiguity resolution strength of (1) and provide explicit links between the model's ambiguity resolution performance and the measurement sampling rate. To this end, we make use of the ADOP. The ADOP is defined as (Teunissen 1997a)

$$\text{ADOP} = \sqrt{|Q_{\hat{a}\hat{a}}|}^{\frac{1}{f(m-1)}} \quad \text{(cycle)}. \tag{12}$$

From the ADOP, one can infer an upper bound for the boot-strapped ambiguity success-rate (Teunissen 2000). The smaller the ADOP, the higher the upper bound of the success-rate becomes. For ADOP smaller than 0.14 cycles, the stated upper bound remains always higher than 99%.

3.1. Single-epoch RTK ADOP as reference

For the sake of comparison, we take the phase-and-code model of single-epoch real-time kinematic (RTK) as reference to analyse the ADOP of the phase-only short-baseline model (1). The corresponding observation equations follow from (1) by sticking to the first epoch $i = 1$ and including the DD observed-minus-computed code measurements $\Delta p_1 \in \mathbb{R}^{f(m-1)}$, that is

$$\begin{cases} \mathsf{E}(\Delta\phi_1) = [\Lambda \otimes I]\, a + [e \otimes G_1]\,\Delta b_1 \\ \mathsf{E}(\Delta p_1) = \qquad\qquad\quad + [e \otimes G_1]\,\Delta b_1 \end{cases}. \tag{13}$$

Compare (1) with (13). With the single-epoch model (13), an ambiguity-float baseline solution can be obtained through the second set of the equations, i.e. the code observation equations.

The phase-and-code RTK model (13) has been widely used in the literature and its ambiguity resolution performance has been studied for several multi-GNSS scenarios (Odolinski *et al* 2015, Brack 2017, Paziewski *et al* 2018). It is therefore important to address how much our phase-only ADOP differs from its rather well-studied RTK counterpart.

Let the positive scalar ε be the phase-to-code variance ratio. The variance matrix of the DD code measurements Δp_1 follows then by dividing the entries of $Q_{\phi_1\phi_1}$, in (3), by ε. The ADOP of the RTK model (13) can be expressed as (Odijk and Teunissen 2008)

$$\text{ADOP}^{\text{RTK}} = \sqrt{2}\, w_o \frac{\sigma_\phi}{\bar\lambda}\Big(1 + \frac{1}{\epsilon}\Big)^{\frac{3}{2f(m-1)}} \tag{14}$$

with $\bar\lambda = \prod_{j=1}^{f} \lambda_j^{\frac{1}{f}}$ and $w_o = \Big(\frac{\sum_{s=1}^{m} w_s}{\prod_{s=1}^{m} w_s}\Big)^{\frac{1}{2(m-1)}}$. To provide insight into (14), let us first make some approximation. The term $\sqrt{2}\, w_o$ is bounded from above by 2 for equal elevation-dependent weights $w^s = 1$ ($s = 1, \ldots, m$). The precision of current GNSS phase data is also about 1% of their wavelength. Thus $(\sigma_\phi/\bar\lambda) \approx 0.01$. Since the code data are almost two orders of magnitude less precise than the phase data (i.e. $\varepsilon \approx 10^{-4}$), the term $(1 + 1/\varepsilon)$ is about 10^4. We therefore arrive at the following approximation

$$\text{ADOP}^{\text{RTK}} \approx 0.02 \times 100^{\frac{3}{f(m-1)}}. \tag{15}$$

When seven satellites ($m = 7$) are tracked, the dual-frequency RTK ADOP is about $0.02 \times 100^{\frac{1}{4}} \approx 0.06$ cycles which is way smaller than 0.14 cycles. This shows, in the absence of code multipath, that single-GNSS, single-epoch ambiguity resolution is possible with the dual-frequency RTK model (13). By switching to the single-frequency case however, the RTK ADOP is about $0.02 \times 100^{\frac{1}{2}} \approx 0.20$ cycles, when $m = 7$. The single-frequency ADOP reduces to about 0.06 cycles if the number of satellites increases to $m = 13$. That is why one has to use multi-GNSS data to achieve successful single-epoch ambiguity resolution with the single-frequency RTK model (Odolinski *et al* 2015).

### 3.2. Dual-epoch phase-only ADOP compared

We now compare the ADOP corresponding to the phase-only model (1) with that of the RTK model (13). The following two phase-only cases are considered:

- *Kinematic*: the case that the unknown baseline vectors b_i ($i = 1, 2$) are assumed fully unlinked in time.
- *Static*: the case that the unknown baseline vector is assumed constant in time, i.e. $b_1 = b_2$;

Lemma 4 (Lemma.). (Phase-only ADOP compared) *Let ADOP^{KIN} and ADOP^{STA} be the ADOPs corresponding to the kinematic and static phase-only models, respectively. These ADOPs can be linked to ADOP^{RTK} in (14) as follows*

Table 2. Information on the GNSS data-sets of the short baseline CUT0–UWA0 as used in the experiment. GPST means 'GPS time'.

	Data (carrier frequencies)	Date	Time	σ_ϕ
10 s data	Galileo(E1/E5a), GPS(L1/L5)	07/Dec/2020	05:40–15:40 GPST	2 mm
1 Hz data	Galileo(E1/E5a), GPS(L1/L5)	07/Dec/2020	05:40–07:20 GPST	2 mm
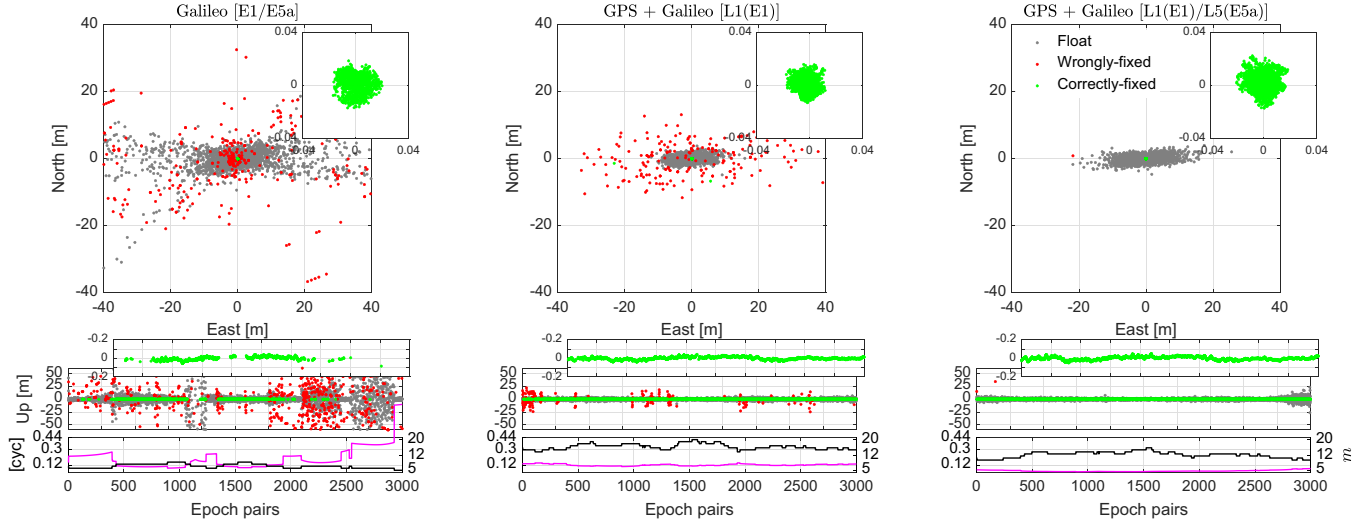
Figure 4. (10 s data-set): East-North position scatter and corresponding Up time-series. At the bottom are shown the ADOP (magenta lines) and number of tracked satellites (black lines) over time. The empirical success-rates, from left to right, are 69.3%, 92.8% and 99.9%, respectively.

$$\frac{ADOP^{KIN}}{ADOP^{RTK}} \approx \frac{1}{\sqrt{2}} \left(\tilde{\epsilon} \, \bar{\gamma} \right)^{\frac{3}{2f(m-1)}}$$

$$\frac{ADOP^{STA}}{ADOP^{RTK}} \approx \frac{1}{\sqrt{2}} \left(\prod_{k=1}^{3} \tilde{\epsilon} \left[1 + \frac{4}{\alpha_k \tau^2} \right] \right)^{\frac{1}{2f(m-1)}}$$

$$\frac{ADOP^{KIN}}{ADOP^{STA}} \approx \left(\frac{1}{\delta} \right)^{\frac{3}{2f(m-1)}} \tag{16}$$

with $\tilde{\epsilon} = \epsilon/(1 + \epsilon)$.

Proof. The proof is given in appendix. □

As the first expression of (16) shows, the ADOP and the baseline's average precision gain (5) are closely intertwined. The smaller the average precision gain $\bar{\gamma}$, the smaller the ADOP becomes (Teunissen 1997a). Also note the presence of the factor $1/\sqrt{2}$ in the first two expressions. The factor indicates that the use of *two epochs* of phase data $\Delta\phi_i$ ($i = 1, 2$), in the phase-only model (1), can decrease the corresponding ADOP. We now focus our attention on the second expression, i.e. the ADOP of the *static* phase-only model. With α_k being of the order of 10^{-8} Hz^2 (figure 1), the second expression can be further approximated for small values of τ as

$$\frac{ADOP^{STA}}{ADOP^{RTK}} \approx \frac{1}{\sqrt{2}} \left(\frac{2}{\tau} \sqrt{\frac{\tilde{\epsilon}}{\alpha}} \right)^{\frac{3}{f(m-1)}}. \tag{17}$$

With the approximation $\sqrt{\tilde{\epsilon}/\alpha} \approx 100$, the above ADOP-ratio is about 10 for the single-frequency case, with a minimum number of seven satellites, when $\tau = 1$ s. This ratio reduces

to about 2.7 for the dual-frequency case and can be further decreased to only 1.1 when the number of satellite increases to $m = 20$.

The last expression of (16) enables us to quantify the extent to which the ADOP-performance of the phase-only model (1) improves by switching from kinematic to static mode. Recall, from figure 1, that the scalar $\sqrt{\delta}$ varies between 0.6 and 1. Thus the last expression approaches its maximum value 1, the larger the numbers of frequencies f and satellites m. Figure 2 shows ADOPs corresponding to models (1) and (13) as functions of the number of satellites m for different sampling periods τ. For both the single- and dual-frequency cases, the gap between the ADOPs of the phase-only kinematic and static models gets smaller when more than eight satellites are tracked. The phase-only ADOPs approach their single-epoch RTK versions, the larger the number of satellites. For the low-rate cases (i.e. 10 and 30 s cases), the dual-frequency phase-only ADOPs gets even smaller than their RTK versions when over 15 satellites are tracked. As with the success-rate results in table 1, our ADOP analysis highlights the capability of the dual-epoch phase-only model (1) for delivering high-precision ambiguity-resolved positioning solutions.

4. Results and discussions

To provide numerical insights into the positioning performance of the dual-epoch phase-only model (1), GPS-plus-Galileo data-sets of a short-baseline, located in Perth, Australia, are analysed. The baseline configuration is shown in figure 3. The underlying carrier signals considered are on
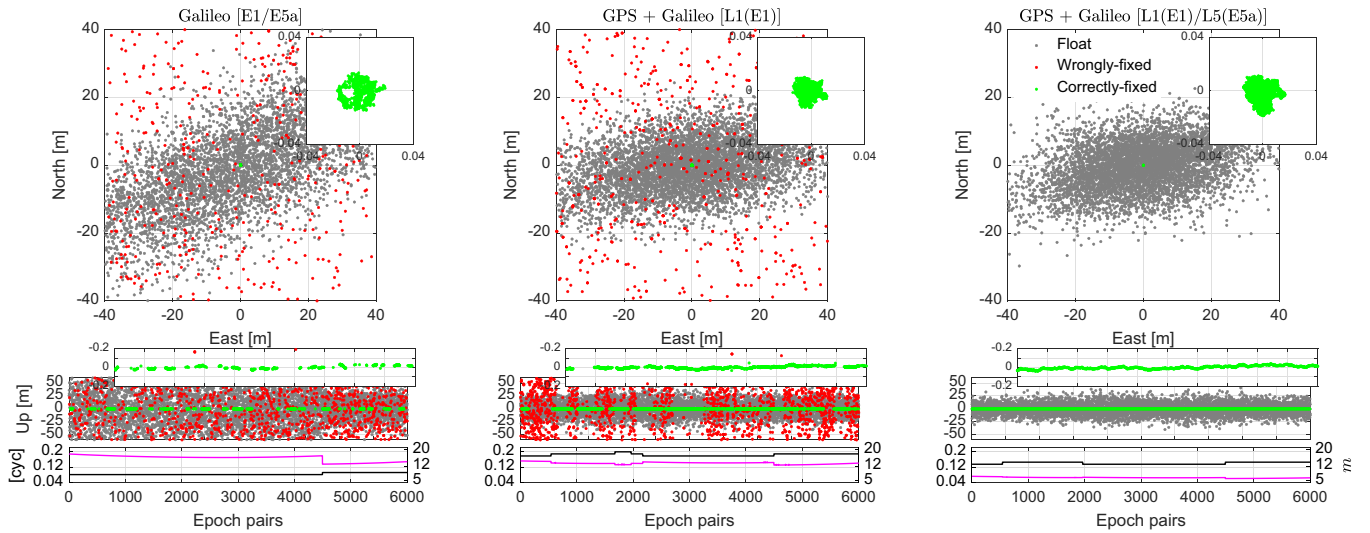
Figure 5. (1 s data-set): East-North position scatter and corresponding Up time-series. At the bottom are shown the ADOP (magenta lines) and number of tracked satellites (black lines) over time. The empirical success-rates, from left to right, are 14.7%, 48.5% and 100%, respectively.
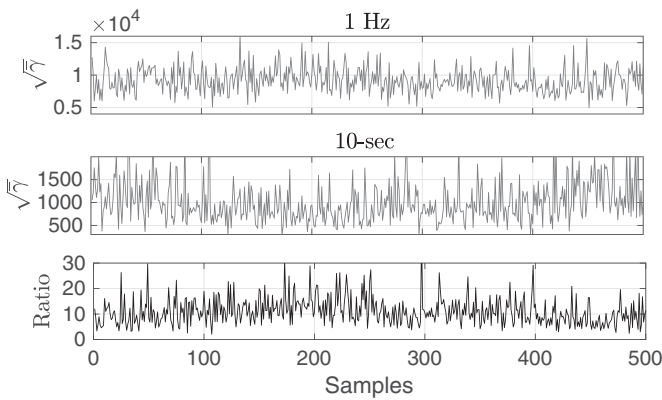
Figure 6. Estimated values of the square-root precision gain $\sqrt{\bar{\gamma}}$ (cf. (5)) for the 1 Hz (top) and 10 s (middle) data-sets, along with the corresponding ratio (bottom).

L1(E1) and L5(E5a) frequencies. Further information about the GNSS data-sets are provided in table 2. As shown in the table, we consider two data-sets of different sampling rates, one with the sampling period of $\tau = 10$ s and the other with $\tau = 1$ s. In both cases, the zenith-referenced standard-deviation of the undifferenced phase measurements is set to be $\sigma_\phi = 2$ mm (cf. equation (3)). To form the satellite elevation-dependent weights w_s in (3), a sinusoidal elevation-weighting strategy is applied as

$$w_s = \sin^2(\theta_s), \quad s = 1, \ldots, m \tag{18}$$

where θ_s ($s = 1, \ldots, m$) are the elevation angles of the satellites commonly tracked by the two receivers.

In figure 4 we show the positioning errors corresponding to the 10 s data-set. The ambiguity-float, correctly-fixed and wrongly-fixed baseline solutions are depicted by grey, green and red dots, respectively. When looking from left to right of the figure, it can be observed how an increase in the

number of frequencies and satellites reduces the number of wrongly-fixed solutions. It should be remarked, for the dual-frequency Galileo case (left), that the solvability condition (2) does not always hold. This is because, in contrast to GPS, the Galileo constellation is not yet fully deployed. We therefore only consider the time-period in which $m \geq 7$. Integrating GPS data, but in a single-frequency mode (middle), the empirical success-rate increases from 69.3% to 92.8%. When the multi-GNSS phase data of the second frequency L5 (E5a) are also used (right), the stated success rate is over 99.9%.

Let us now consider the phase-only positioning performance for the 1 Hz data-set. The corresponding results are shown in figure 5. As predicted by the formal results in table 1, we observe a considerable drop in the ambiguity success-rate upon decreasing the sampling period from $\tau = 10$ s to $\tau = 1$ s. Only 14.7% of the dual-frequency Galileo solutions (left) are correctly fixed. This number increases to 48.5% for the single-frequency GPS-Galileo case. In case of the dual-frequency multi-GNSS phase data however, *all* the solutions are correctly fixed, leading to cm-level positioning solutions. This is expected as the corresponding ADOP is well below 0.14 cycles.

To conclude this section, we verify the impact the choice of the sampling period τ has on the baseline precision gain. A comparison between the two figures 4 and 5 (right-panels) reveals that the dispersion of the ambiguity-float solutions gets considerably larger by decreasing the sampling period from $\tau = 10$ s to $\tau = 1$ s. The dispersion of the correctly-fixed solution remains almost unchanged. Using the positioning errors in the East, North and Up directions, we estimate the float and fixed baseline variance matrices $Q_{\hat{b}_i \hat{b}_i}$ and $Q_{\check{b}_i \check{b}_i}$ for about 500 samples to numerically evaluate the average precision gain $\bar{\gamma}$ in (5). The corresponding square-root values are presented in figure 6. As predicted by the formal result (8), the square-root gain $\sqrt{\bar{\gamma}}$ is of the orders of 10^4 and 10^3 for the 10 s ($\tau = 10$ s) and 1 Hz ($\tau = 1$ s) sampling rates, respectively. As illustrated in the bottom-panel of the figure, the corresponding ratio of the two stated square-root gains fluctuates around 10 which

is identical to the ratio of their underlying sampling-rates (i.e. 1 Hz over 0.1 Hz).

5. Concluding remarks and outlook

In this contribution we studied the positioning performance of the dual-epoch phase-only model (1). Closed-form expressions for the variance matrices of the corresponding parameter solutions were derived and the extent to which the baseline precision can be improved by successful ambiguity solution was quantified. In case of 1 Hz GNSS phase measurements, the ambiguity-float baseline precision is about tens of metres. The corresponding standard deviation is inversely proportional to the measurements' sampling rate (cf. (8)). Thus by decreasing the sampling rate to 0.1 Hz (10 s), the stated precision improves to several metres which is still way poorer than the sub-centimetre precision obtained by its fixed counterpart.

In the proposed phase-only model, the unknown baselines of the two involved epochs are treated as *fully* unlinked-in-time parameters. Such 'kinematic' model is therefore weaker than that of its 'static' counterpart in which the baseline is assumed to behave constant in time. It was, both analytically and numerically, demonstrated that such model's weakness is not of practical relevance for a multi-GNSS landscape (cf figure 2). A modest increase in the number of tracked satellites, that can be brought by a multi-GNSS integration, makes the ambiguity-resolution performance of the kinematic phase-only model almost the same as that of its static version. With the use of multi-GNSS high-rate phase data of two successive epochs, one can therefore deliver near real-time cm-level ambiguity-resolved positioning solutions (figure 5).

With the proven positioning capability of model (1), it is foreseen that the applicability of phase-only positioning will be extended to observable carrier phase signals that are broadcast by low earth orbit satellite communication systems (Khalife *et al* 2020).

In this study, attention was focused on the precision of the phase-only model's parameter solutions. A study on the testing procedures with which one can ensure the model's integrity against potential modelling errors, such as phase cycle slips (Khodabandeh and Teunissen 2015b, Zaminpardaz and Teunissen 2019), is the topic of future works.

Data availability statement

Acknowledgment

Appendix A.

Proof of Lemmas (1) and (3). With the stochastic model (3), the least-squares normal matrix of (1) follows as

$$N = \left[\begin{array}{cc} N_{aa} & N_{ab} \\ N_{ab}^T & N_{bb} \end{array} \right] \quad (A.1)$$

with

$$\begin{array}{rcl} N_{aa} & = & \frac{1}{2\sigma_\phi^2} \Lambda^2 \otimes (W_1 + W_2) \\ N_{ab} & = & \frac{1}{2\sigma_\phi^2} \sum_{i=1}^{2} u_i^T \otimes \Lambda e \otimes W_i G_i \\ N_{bb} & = & \frac{f}{2\sigma_\phi^2} \sum_{i=1}^{2} u_i u_i^T \otimes G_i^T W_i G_i \end{array} \quad (A.2)$$

where $u_1 = [1,0]^T$ and $u_2 = [0,1]^T$. The ambiguity variance matrix (11) follows from the inversion of the reduced normal matrix

$$\begin{aligned} Q_{\hat{a}\hat{a}}^{-1} &= N_{aa} - N_{ab} N_{bb}^{-1} N_{ab}^T \\ &= \frac{1}{\sigma_\phi^2} \left\{ \Lambda \mathcal{P}_e^\perp \Lambda \otimes W + \frac{1}{2} \Lambda \mathcal{P}_e \Lambda \otimes \sum_{i=1}^{2} W_i \mathcal{P}_{G_i}^\perp \right\}, \quad \text{(A.3)} \end{aligned}$$

as $(W_1 + W_2) = 2W$. The fixed baseline variance matrix in (4) is directly obtained by the inversion of N_{bb}, as the ambiguities (and therefore both N_{aa} and N_{ab}) are absent for the fixed case. Thus $(\check{b} = [\check{b}_1^T, \check{b}_2^T]^T)$

$$\begin{array}{rcl} Q_{\check{b}\check{b}} & = & N_{bb}^{-1} \\ & = & \frac{2\sigma_\phi^2}{f} \sum_{i=1}^{2} u_i u_i^T \otimes (G_i^T W_i G_i)^{-1}. \end{array} \quad (A.4)$$

Finally, the float baseline variance matrix in (4) is obtained from the following matrix-inversion identity $(\hat{b} = [\hat{b}_1^T, \hat{b}_2^T]^T)$

$$Q_{\hat{b}\hat{b}} = N_{bb}^{-1} + N_{bb}^{-1} N_{ab}^T Q_{\hat{a}\hat{a}} N_{ab} N_{bb}^{-1}. \quad (A.5)$$

$\square$

Proof of Lemma (2). Suppose $W_2 \approx W_1 = W$. From (A.2), the inverse of the float and fixed baseline variance matrices follow as

$$\begin{aligned} Q_{\hat{b}\hat{b}}^{-1} &= \frac{f}{4\sigma_\phi^2} \left[\begin{array}{cc} +G_1^T W G_1, & -G_1^T W G_2 \\ -G_2^T W G_1, & +G_2^T W G_2 \end{array} \right] \\ Q_{\check{b}\check{b}}^{-1} &= \frac{f}{2\sigma_\phi^2} \left[\begin{array}{cc} +G_1^T W G_1, & 0 \\ 0, & +G_2^T W G_2 \end{array} \right]. \end{aligned} \quad (A.6)$$

Pre- and post-multiplying the above matrices by

$$L = \left[\begin{array}{cc} I, & I \\ -I, & I \end{array} \right], \quad (A.7)$$

and its transpose gives

$$LQ_{\hat{b}\hat{b}}^{-1}L^T = \frac{f}{4\sigma_\phi^2}\begin{bmatrix} G_{12}^T WG_{12}, & 2G_{12}^T WG \\ 2G^T WG_{12}, & 4G^T WG \end{bmatrix}$$

$$LQ_{\check{b}\check{b}}^{-1}L^T = \frac{f}{2\sigma_\phi^2}\begin{bmatrix} \sum_{i=1}^2 G_i^T WG_i, & G_2^T WG_2 - G_1^T WG_1 \\ G_2^T WG_2 - G_1^T WG_1, & \sum_{i=1}^2 G_i^T WG_i \end{bmatrix}$$
(A.8)

with $2G = (G_1 + G_2)$ and $G_{12} = G_2 - G_1$. Substitution of $\sum_{i=1}^2 G_i^T WG_i = 2G^T WG + (1/2)G_{12}^T WG_{12}$, $G_{12} \approx \tau\dot{G}$ and $G_2^T WG_2 - G_1^T WG_1 \approx \tau(\dot{G}^T WG + G^T W\dot{G})$ into (A.8), together with an application of the determinant factorization rule (Koch 1999), gives

$$\begin{aligned}
\frac{|Q_{\hat{b}\hat{b}}|}{|Q_{\check{b}\check{b}}|} &= \frac{|LQ_{\check{b}\check{b}}^{-1}L^T|}{|LQ_{\hat{b}\hat{b}}^{-1}L^T|}\\
&= \frac{|G^T WG + (\tau/2)^2 \dot{G}^T W\dot{G}|}{|(\tau/2)^2 \dot{G}^T W\dot{G}|}\\
&\quad \times \frac{|G^T WG + (\tau/2)^2 \dot{G}^T W\dot{G}|}{|G^T WG - G^T W\mathcal{P}_{\dot{G}}G|}\\
&\quad \times |I - (\tau/2)^2 X^{-1}Y X^{-1}Y|
\end{aligned}$$
(A.9)

with $X = G^T WG + (\tau/2)^2 \dot{G}^T W\dot{G}$ and $Y = (\dot{G}^T WG + G^T W\dot{G})$. From the definition of the generalized eigenvalues (Teunissen 1997a), as given in (7), follows that

$$\frac{|G^T WG + (\tau/2)^2 \dot{G}^T W\dot{G}|}{|(\tau/2)^2 \dot{G}W\dot{G}|} = \prod_{k=1}^3\left[1 + \frac{(2/\tau)^2}{\alpha_k}\right]$$

$$\frac{|G^T WG + (\tau/2)^2 \dot{G}^T W\dot{G}|}{|G^T WG - G^T W\mathcal{P}_{\dot{G}}G|} = \frac{\prod_{k=1}^3[1 + (\tau/2)^2\alpha_k]}{\prod_{k=1}^3[1 - \beta_k]}.$$
(A.10)

In case of GNSS, the entries of $X^{-1}Y$ are of the order of 10^{-4}, meaning that the last term in (A.9) is almost equal to 1. For small values of τ, we have $|Q_{\hat{b}\hat{b}}|/|Q_{\check{b}\check{b}}| \approx |Q_{\hat{b}_i\hat{b}_i}|/|Q_{\check{b}_i\check{b}_i}|$. Thus the first expression of (6) follows by substituting (A.10) into (A.9), while the second expression follows by neglecting the presence of quantities compared to the terms $(1/\alpha_k)$ ($k = 1, 2, 3$). $\qquad\square$

Proof of Lemma (4). The proof follows from the determinant rule (Odijk and Teunissen 2008):

$$|Q_{\hat{a}\hat{a}}| = |N_{aa}^{-1}|\frac{|Q_{\hat{b}\hat{b}}|}{|Q_{\check{b}\check{b}}|},$$
(A.11)

together with (A.9) and (A.10), and ADOP-results in Teunissen (1997a). $\qquad\square$

ORCID iD

A Khodabandeh ● https://orcid.org/0000-0002-5051-8233

References

Blewitt G 1989 Carrier phase ambiguity resolution for the global positioning system applied to geodetic baselines up to 2000 km *J. Geophys. Res.* **94** 10187–203

Brack A 2017 Reliable GPS+BDS RTK positioning with partial ambiguity resolution *GPS Solut.* **21** 1083–92

Codol J M and Monin A 2011 Improved triple difference GPS carrier phase for RTK-GPS positioning *2011 IEEE Statistical Signal Processing Workshop (SSP)* (IEEE) pp 61–4

Gunther C and Henkel P 2012 Integer ambiguity estimation for satellite navigation *IEEE Trans. Signal Process.* **60** 3387–93

Han S 1997 Quality-control issues relating to instantaneous ambiguity resolution for real-time GPS kinematic positioning *J. Geod.* **71** 351–61

Hassibi A and Boyd S 1998 Integer parameter estimation in linear models with applications to GPS *IEEE Trans. Signal Process.* **46** 2938–52

Hauschild A, Grillmayer G, Montenbruck O, Markgraf M and Vörsmann P 2008 *GPS Based Attitude Determination for the Flying Laptop Satellite* (Dordrecht: Springer Netherlands) pp 211–20

Henderson H V, Pukelsheim F and Searle S R 1983 On the history of the Kronecker product *Linear Multilinear Algebr.* **14** 113–20

Hobiger T, Sekido M, Koyama Y and Kondo T 2009 Integer phase ambiguity estimation in next-generation geodetic very long baseline interferometry *Adv. Space Res.* **43** 187–92

Huisman L, Teunissen P J G and Odijk D 2010 On the robustness of next generation GNSS phase-only real-time kinematic positioning *Proc. FIG Congress* (Sydney)

Jonkman N F, Teunissen P J G, Joosten P and Odijk D 2000 GNSS long baseline ambiguity resolution: impact of a third navigation frequency *IAG Symp. 121, Geodesy Beyond 2000* (Springer) pp 349–54

Kampes B M and Hanssen R F 2004 Ambiguity resolution for permanent scatterer interferometry *IEEE Trans. Geosci. Remote Sens.* **42** 2446–53

Khalife J, Neinavaie M and Kassas Z M 2020 Navigation with differential carrier phase measurements from megaconstellation LEO satellites *2020 IEEE/ION Position, Location and Symp. (PLANS)* pp 1393–404

Khodabandeh A and Teunissen P J G 2015a An analytical study of PPP-RTK corrections: precision, correlation and user-impact *J. Geod.* **89** 1109–32

Khodabandeh A and Teunissen P J G 2015b Single-Epoch GNSS array integrity: an analytical study *VIII Hotine-Marussi Symposium on Mathematical Geodesy* (Springer) pp 263–72

Khodabandeh A and Teunissen P J G 2018 On the impact of GNSS ambiguity resolution: geometry, ionosphere, time and biases *J. Geod.* **92** 637–58

Koch K R 1999 *Parameter Estimation and Hypothesis Testing in Linear Models* (Berlin: Springer)

Montenbruck O *et al* 2017 The Multi-GNSS Experiment (MGEX) of the Int. GNSS Service (IGS)–achievements, prospects and challenges *Adv. Space Res.* **59** 1671–97

Odijk D and Teunissen P J G 2008 ADOP in closed form for a hierarchy of multi-frequency single-baseline GNSS models *J. Geod.* **82** 473–92

Odolinski R, Teunissen P J G and Odijk D 2015 Combined BDS, Galileo, QZSS and GPS single-frequency RTK *GPS Solut.* **19** 151–63

Paziewski J, Sieradzki R and Baryla R 2018 Multi-GNSS high-rate RTK, PPP and novel direct phase observation processing method: application to precise dynamic displacement detection *Meas. Sci. Technol.* **29** 035002

Remondi B W 1989 *Using the Global Positioning System (GPS) Phase Observable for Relative Geodesy: Modeling, Processing and Results* (Austin, TX: U.S. Department of Commerce,

National Oceanic and Atmospheric Administration, National Ocean Service)

Remondi B W and Brown G 2000 Triple differencing with Kalman filtering: making it work *GPS Solut.* **3** 58–64

Teunissen P J G 1995 The least-squares ambiguity decorrelation adjustment: a method for fast GPS integer ambiguity estimation *J. Geod.* **70** 65–82

Teunissen P J G 1997a A canonical theory for short GPS baselines. Part I: the baseline precision *J. Geod.* **71** 320–36

Teunissen P J G 1997b GPS double difference statistics: with and without using satellite geometry *J. Geod.* **71** 137–48

Teunissen P J G 1999 An optimality property of the integer least-squares estimator *J. Geod.* **73** 587–93

Teunissen P J G 2000 ADOP based upper bounds for the bootstrapped and the least squares ambiguity success *Artif. Satell.* **34** 171–9

Teunissen P J G, de Jonge P J and Tiberius C C J M 1997 The least-squares ambiguity decorrelation adjustment: its performance on short GPS baselines and short observation spans *J. Geod.* **71** 589–602

Teunissen P J G, Simons D G and Tiberius C C J M 2005 *Probability and Observation Theory* (Faculty of Aerospace Engineering, Delft University of Technology: Delft University) (Lecture Notes AE2-E01)

Tiberius C C J M and de Jonge P J 1995 Fast positioning using the LAMBDA method *Proc. 4th Int. Symp. on Differential Satellite Navigation Systems (Bergen, Norway, 24–28 April)* vol 30 (Citeseer)

Verhagen S, Li B and Teunissen P J G 2013 Ps-LAMBDA: ambiguity success rate evaluation software for interferometric applications *Comput. Geosci.* **54** 361–76

Viegas D and Cunha S R 2007 Precise positioning by phase processing of sound waves *IEEE Trans. Signal Process.* **55** 5731–8

Wang K, Chen P and Teunissen P J G 2018 Fast phase-only positioning with triple-frequency GPS *Sensors* **18** 3922

Xu P, Shi C and Liu J 2012 Integer estimation methods for GPS ambiguity resolution: an applications oriented review and improvement *Surv. Rev.* **44** 59–71

Zaminpardaz S and Teunissen P J G 2019 DIA-datasnooping and identifiability *J. Geod.* **93** 85–101